Article

The Performance and Mechanism of the Green Explosion Suppressant SGA for Coal Dust Explosion Suppression

Yansong Zhang, Kun Chen, Junjie Yang, Jinshe Chen,* Zhichao Pan, Wenxi Shi, Xiangbao Meng, Xinyan Zhang, and Min He

Cite This: ACS Omega 2021, 6, 35416−35426

Read Online

ACCESS | Metrics & More | Article Recommendations

ABSTRACT: In recent years, coal processing is developing rapidly, but there are often hidden safety hazards such as coal dust explosions during coal processing. In order to ensure safe production and avoid coal dust explosion accidents, a carrier with unique micro-mesoporous structure (SG) based waste molecular sieves was prepared. After that, the carrier was loaded with $(NH_4)_2C_2O_4(A)$ uniformly by ultrasound, which acted as an activity component for the first time. A novel micro-mesoporous coal dust explosion suppressant (SGA) is obtained. The law influence of different compositions of suppressant on the flame propagation of explosion was investigated. The results showed that the best ratio of waste molecular sieve, zirconium dioxide, and $(NH_4)_2C_2O_4$ of the suppressant is 1:7:2. The suppression performance increases with the increase of the addition of suppressant. When the addition amount is 70 wt %, the explosion loses the ability to continue to expand. Finally, combining the suppression performance with characterization results, the physical and chemical synergistic suppression mechanism is proposed, which reveals the reason why the suppressant has efficient suppression performance. The study could realize the green reuse of waste molecular sieves and provide guarantees for safe production of the coal processing industry.
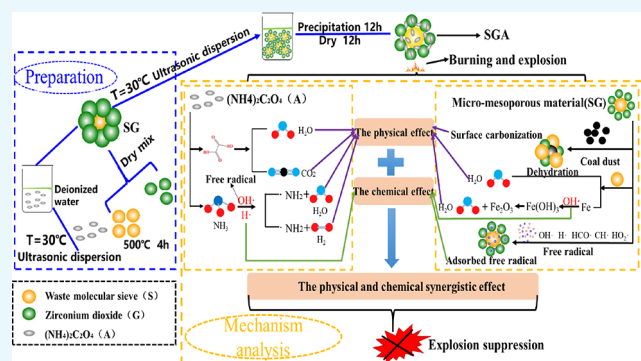
1. INTRODUCTION

The coal chemical industry, in which coal is used as a raw material, accounts for approximately 60% of the total energy production of China. A lot of coal dusts are produced in industrial processes, including transporting, storing, crushing, and grinding of coal.[1−5] Especially, the obvious yet hidden danger of coal dust explosions exists in the equipment, which seriously threatens the safety and production of industrial coal processes.[6] Coal dusts, which are relatively light, can easily become airborne and remain aloft in enclosed and semi-enclosed spaces to form dust clouds. When dust clouds are exposed to a spark, they can be ignited and rapidly accelerate into an explosion, causing a large-scale catastrophe.[7−10] Moreover, the raw coal processed in the coal chemical industry typically has coal dust with a small particle size, which has low explosion concentration and ignition temperature. Additionally, the environment of coal chemical industry is usually high temperatures and pressures, and explosions caused by the leakage of coal dust could easily occur. These explosions have resulted in numerous deaths, injuries, and massive economic losses.[11−13]

In an effort to prevent and control coal dust explosions, researchers have mainly focused their studies on flame-proofing and explosion suppression.[14−18] Because of their low cost and ease of transportation, powder suppressants have been widely used. Explosion suppression with rock powders has been used extensively because of their low cost.[19] However, their explosion suppression performance is unsatisfactory, with the only effect of physical explosion suppression.[20] The effectiveness of other explosion suppressants has been better, but some problems still exist, including high cost and insufficient performance. The study of a low-cost, high-performance suppressant is important to prevent coal dust explosions. Cheng et al.[21] investigated the suppression of gas explosions by diatomite and quartz powders. Their results indicated that diatomite powder is more effective in explosion suppression than quartz powder and the explosion suppression performance is closely related to the hydroxyl content and porous structure on the surface of diatomite
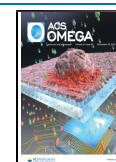
powder. Yu et al.[22] have studied the characteristic parameters of pyrolysis of a variety of powder suppressants, including $Al(OH)_3$, $Mg(OH)_2$, and carbamide. They reported that the explosion suppression performance of carbamide is better than those of $Al(OH)_3$ and $Mg(OH)_2$. Their analysis of the explosion suppression mechanism shows that a great amount of $NH_4\cdot$ and $NCO\cdot$ are produced in the pyrolysis of carbamide, which react with the $H\cdot$ and $OH\cdot$ active radicals, respectively, decreasing the quantity of radicals and thereby terminating the chain reaction of the explosion. Yuan et al.[23] have investigated the suppression effect of a porous mineral (MTS)−ammonium polyphosphate (APP) composite powder on the explosion of methane and air. Their results showed that the explosion suppression mechanism of the composite powder includes both physical and chemical suppression. The complicated structure of MTS could improve the capture ability of radicals. Additionally, the successively occurring pyrolysis of MTS and APP continuously absorbs heat, and the decomposition products have the effect of attenuating, cooling, isolating, and largely consuming the free radicals.

Molecular sieves are a kind of synthetic hydrated silicate aluminate with porous structures that have the advantages of good adsorption and selectivity.[24−26] They are widely used in the organic chemical industry, the petrochemical industry, and exhaust purification. However, the activity of a molecular sieve gradually decreases and finally disappears during continuous use. A large deal of industrial waste molecular sieve was produced throughout the world.[27−29] As the industry rapidly develops, the amount of waste molecular sieve produced gradually increases. According to statistics, the yearly global output of waste molecular sieve is as high as 0.5−0.7 million tons. They are primarily microporous molecular sieves that have little catalytic activity and are harmful to the environment. Every year, a great amount of capital is consumed in their disposal, which increases the cost of production.[30−33] Molecular sieves have a uniform cellular structure and good hydrothermal stability, but their pore diameter limits effective loading of active components. Especially, for waste molecular sieves, their pore structures are partially blocked and unfit for loading active components. Moreover, there are Fe, V, and Ni elements in waste molecular sieves, particularly a certain amount of Fe element. How to reuse waste molecular sieves into materials with high added value has becomes a crucial problem faced by many enterprises.[34−37]

Mesoporous materials have relatively large pore diameters, and the pores are easily used to load more active components. Liu et al.[38] used a sol−gel method to prepare Ni/CaO-ZrO$_2$ with high heat stability. Their results showed that CaO enhanced the alkalinity of the catalyst, promoting the chemical adsorption and dissociation of CO_2. Feng[39] used ZrO_2 with different porous structures to load gold nanoparticles as catalysts. They studied the effect of light intensity and wavelength on the reaction and analyzed the effect of the porous structure of the ZrO_2 carrier on the catalytic activity. Their results showed that a change of light intensity and wavelength of visible light influenced the reaction. It was observed that the mesoporous materials were useful to load the active component. The green use of waste molecular sieves could be achieved when waste molecular sieves with a micropore structure are combined with ZrO_2 to prepare a novel material for explosion suppression, which would be significant scientifically and technologically. With $(NH_4)_2C_2O_4$ as an active component, NH_3 and CO_2 gas can be released by

it, which is in favor of explosion suppression. However, there are no studies on the use of $(NH_4)_2C_2O_4$ in explosion suppression of coal dust.

In this work, the green recycling of waste molecular sieves was achieved by combining waste molecular sieves with a microporous structure and ZrO_2 with a mesoporous structure. Especially, $(NH_4)_2C_2O_4$ was used as the active component for explosion suppression for the first time. The mesoporous structure in the suppressant contributed to the high efficiency of the loading active component $(NH_4)_2C_2O_4$. In addition, the mesoporous structure in the suppressant was in favor of rapid entry of the flame in the explosion process. The agglomeration of the active component was solved by the successful loading of $(NH_4)_2C_2O_4$ on micro-mesoporous materials. Simultaneously, inert gas generated by $(NH_4)_2C_2O_4$ during the explosion suppression process could dilute oxygen. The micro-mesoporous material has a specific pore structure and metal elements such as Fe etc., which is helpful for adsorbing mass of free radicals of explosion . The effect of the suppressant on the flame propagation law and its performance of explosion suppression were investigated. Combing with the characterization results, it indicates that the micro-mesoporous suppressant has efficient synergistic effect of physics and chemistry in coal dust explosion suppression. This work can not only realize the green reuse with high added value of waste molecular sieves but also provide guarantees for safe production of the coal processing industry.

2. RESULTS AND DISCUSSION

2.1. Characterization of Samples. Figure 1 shows the SEM images of S, G, SG, and SGA. As shown in the scanning
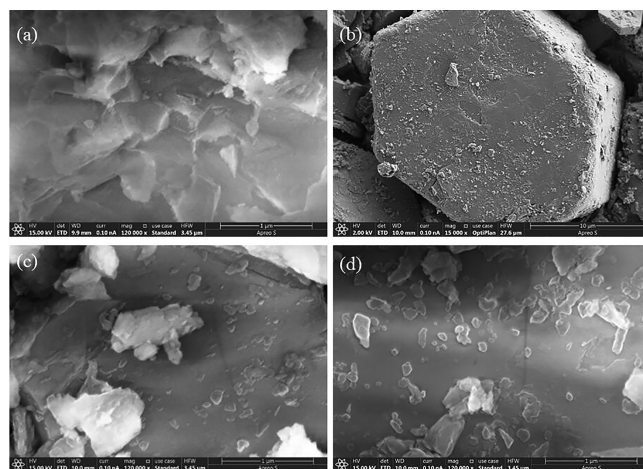

Figure 1. SEM images of (a) S, (b) G, (c) SG, and (d) SGA.

electron microscopy (SEM) image in Figure 1a, S had an irregular bulk shape, and parts of its surface were porous. Figure 1b shows that G also had an irregular bulk shape. The mixed material of S and G still showed an irregular bulk shape in Figure 1c. After the loading of component A, SEM revealed that the material still possessed an irregular bulk shape, and small particles are observed in Figure 1d, indicating that active component was successfully loaded on the micro-mesoporous carrier.

Energy dispersive X-ray spectroscopy (EDS) was used to characterize the elemental composition of the materials, as shown in Figure 2. S and SGA composite contained Fe, Ni, and
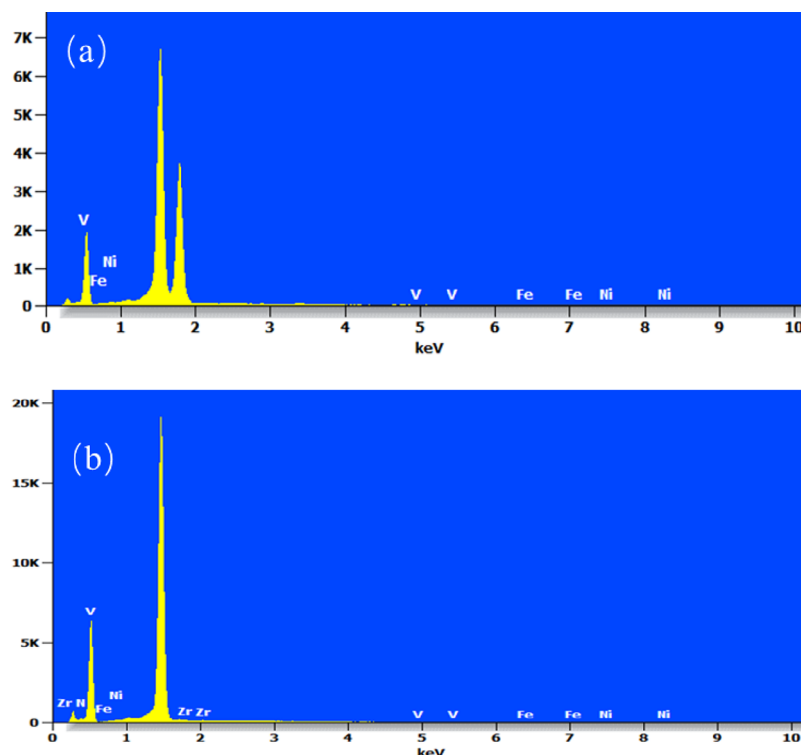
Figure 2. EDS spectra of (a) S and (b) SGA.

V. However, the SGA composite also contained Zr and N. The existence of Zr indicated the presence of G, and the existence of N indicated the presence of A. Hence, a suppressant containing S, G, and A was successfully prepared.

The distribution of elements V, Fe, and Ni was quite uniform, as shown in the SEM mapping image in Figure 3. The uniformity demonstrated that S was dispersed uniformly in the

Figure 3. SEM mapping image of SGA.

suppressant. Also, the uniform distribution of elements Zr and N demonstrated a uniform distribution of components G and A in the suppressant. Therefore, each component was well dispersed in the novel suppressant, which was prepared by the dry mixing method.

The X-ray diffraction (XRD) peaks belonging to molecular sieve Y at 2θ = 10.41, 12.19, 15.99, 20.70, 24.05, 45.90, and 66.78° appeared in the XRD of S, as shown in Figure 4a, indicating that the molecular sieve Y was mainly contained in S.[40] Figure 4b shows that diffraction peaks appear at 2θ = 18.45, 20.46, 27.08, 36.78, 37.93, 44.41, 54.56, and 63.29°, and these diffraction peaks are attributed to cubic zirconia.[41] Additionally, some XRD peaks of S and G appeared in the XRD of the suppressant shown in Figure 4c, which proved that S and G were contained. However, as the S/G mass ratio in the sample was 1:7, the diffraction peak of G was relatively strong, while the diffraction peak of S was relatively weak due to low content in micro-mesoporous (SG). The XRD peaks of SGA appeared at 2θ = 24.80 and 33.72°, as shown in Figure 4d, indicating that A was successfully loaded on the micro-mesoporous carrier.[42]

The specific surface area and total pore volume of S were 90 m^2/g and 0.02 cm^3/g, respectively. The specific surface area and total pore volume of micro-mesoporous (SG) significantly decreased after dry mixing, as shown in Table 1. The decrease was due to the effect of the merging and coverage of G on the pores of S. Clearly, the specific surface area and total pore volume of SGA significantly decreased with the loading of A, which indicated that the pore was gradually filled with A and A was loaded on SG successfully.

The adsorption−desorption isotherm of N_2 in S was type IV isotherm, as shown in Figure 5. When the relative pressure P/P_0 was <0.1, the adsorbing capacity of N_2 increased rapidly, which suggested the existence of the micropores in S. A hysteresis loop of type H4 occurred when P/P_0 = 0.4−1,

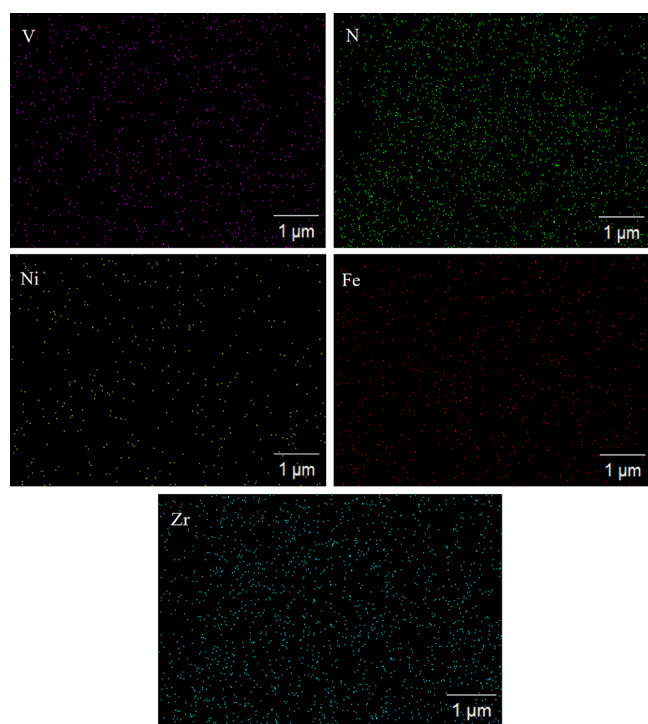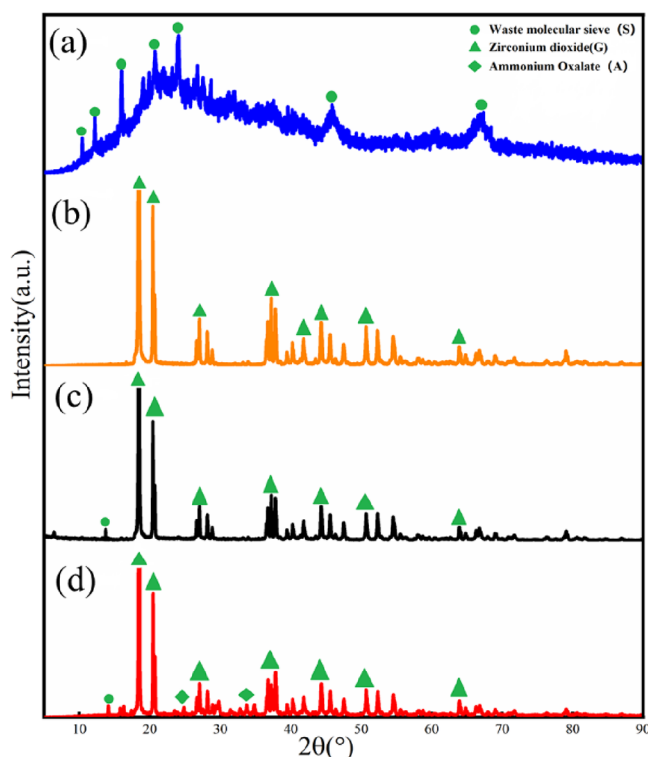**Figure 4.** XRD patterns of (a) S, (b) G, (c) SG, and (d) SGA.

Table 1. BET of S, SG, and SGA

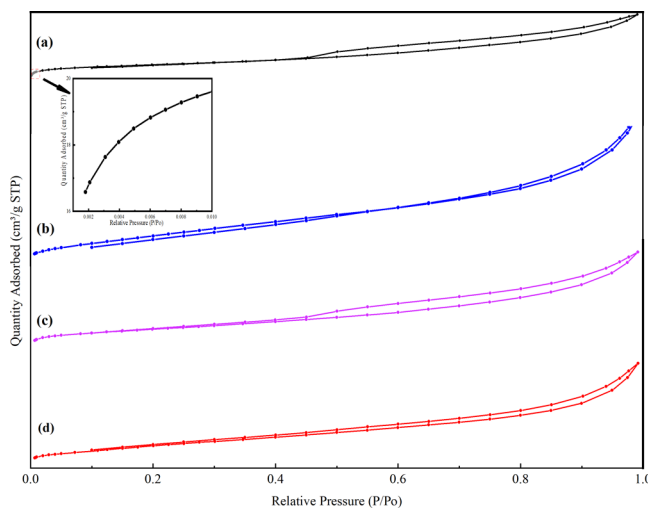| sample	BET (m^2/g)	VT (cm^3/g)	d mesopore
S	90.3557	0.020953	7.7879
SG	15.7313	0.001785	7.7956
SGA	6.7231		7.3414

Figure 5. Adsorption curve of (a) S, (b) G, (c) SG, and (d) SGA.

indicating that some mesoporous or macroporous structures exist because S has been used for a long time in production. The adsorption−desorption isotherm of N$_2$ in G was also a type IV isotherm, and the adsorption at low P/P_0 had the same basic characteristics as the mesoporous material. In contrast, when P/P_0 = 0.8−1, the occurrence of a type H4 hysteresis loop implied the existence of a mesoporous or macroporous structure. The adsorption−desorption isotherms of N$_2$ in the

carrier micro-mesoporous (SG) and SGA were both type IV isotherms, and the adsorption capacity of N$_2$ increased rapidly in micro-mesoporous (SG) when P/P_0 was 0.2−1. A type H4 hysteresis loop occurred, which indicated that the carriers all had a mesoporous structure. However, compared with the adsorption isotherm of the carrier micro-mesoporous (SG), the hysteresis loop of SGA became smaller, suggesting that the carrier was gradually filled with A after the loading of A.

The pore diameter size of S was mainly 1 nm, and that of G was in the ranges of 2, 5, 10, 20, and 40 nm shown in Figure 6a,b. As S and G were mixed at a ratio of 1:7, the pore
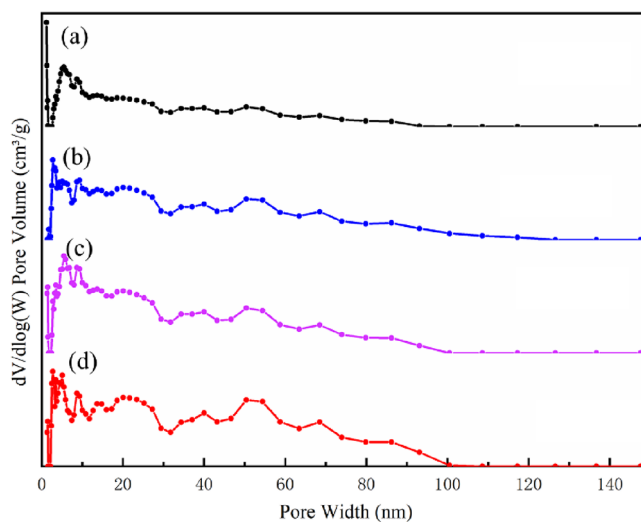

Figure 6. Pore size distribution of (a) S, (b) G, (c) SG, and (d) SGA.

diameter size was in the ranges of 1, 5, 10, 20, and 40 nm, as shown in Figure 6c. When the loading of A was 20 wt %, the peak intensity at 1 nm weakened, which indicated that A was first loaded into the micropore structure of the micro-mesoporous suppressant.

The TG curve of S in Figure 7a revealed that S slightly lost weight before reaching 200 °C, which was caused by the desorption of a small amount of water in S. In general, there was no obvious weight loss in the TG curve of S, indicating that S had relatively high thermal stability. The TG curve of SG in Figure 7b contained two stages including rapid and slow weight loss. Pyrolysis occurred at 200 °C. The TG curve started to decrease, and the rate of weight loss slowed, which resulted from the decomposition of impurities in S and G. The stage of slow weight loss began at 300 °C, which might have resulted from the solid solution phenomenon caused by a small amount of Al$_2$O$_3$ in S acting as a stabilizer of zirconium oxide. The TG curve of SG no longer decreased at 550 °C. The pyrolysis in the TG curve of SGA shown in Figure 7c was mainly divided into five stages. In stage 1, slow weight loss occurred over 60−100 °C with a weight loss ratio of 4%, mainly due to the desorption of a small amount of water in the suppressant and the decomposition of a small amount of A. In stage 2, weight loss occurred over 100−220 °C with a weight loss ratio of 10%, and oxalic acid decomposed at about 195 °C. In stage 3, rapid weight loss occurred over 220−300 °C with a weight loss ratio of 25%, which resulted from the decomposition of impurities in S and G. In stage 4, slow weight loss occurred over 300−360 °C with a weight loss ratio of 9%, which resulted from the solid solution phenomenon
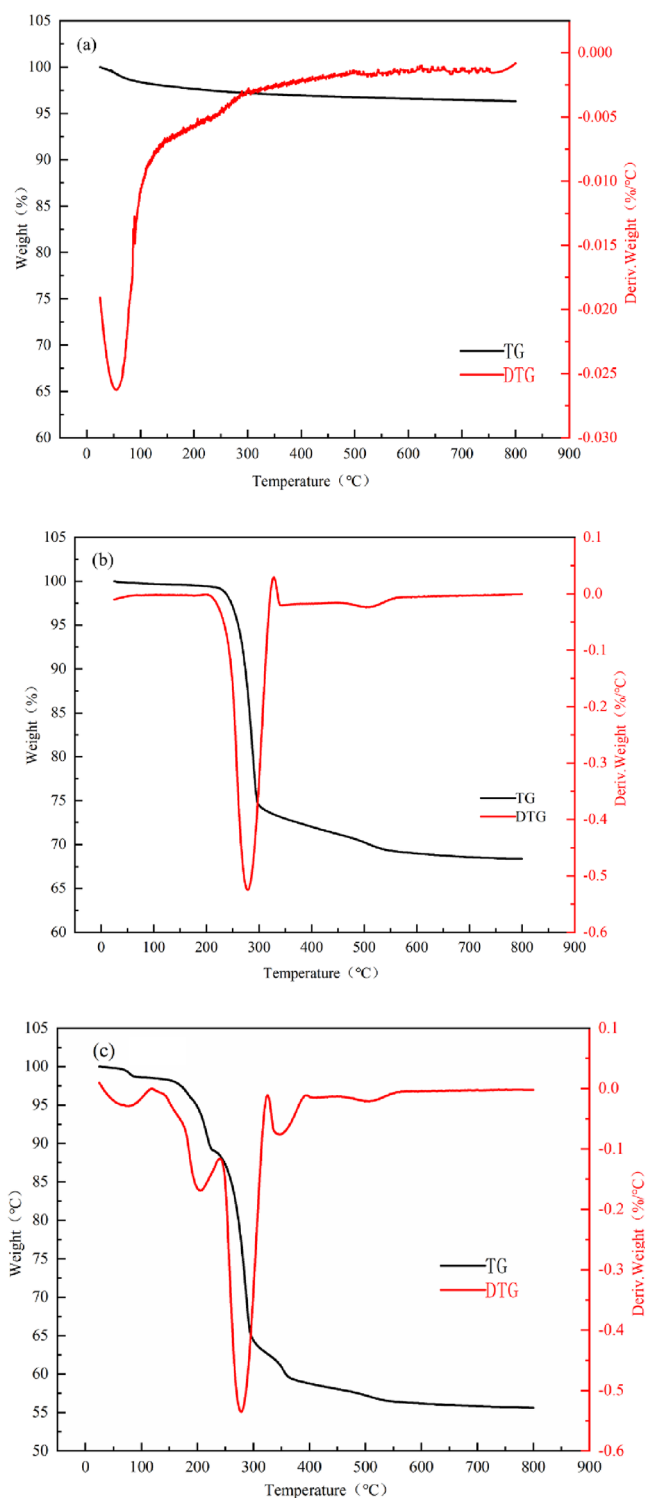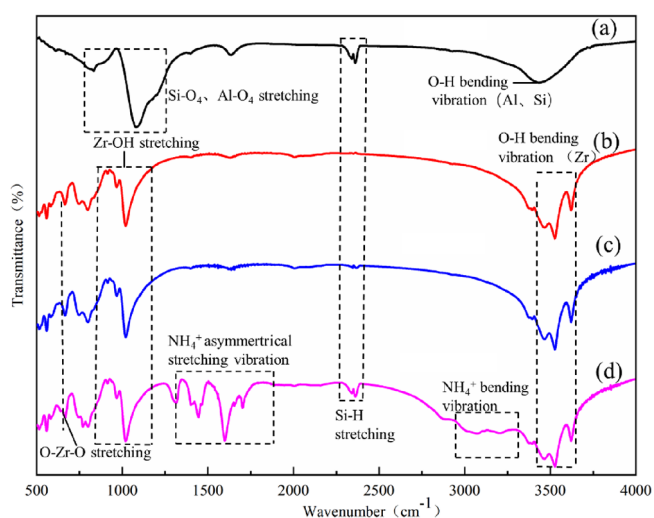
Figure 8. FTIR of (a) S, (b) G, (c) SG, and (d) SGA.

appeared in the FTIR spectra of SG and SGA, which indicated that both SG and SGA contained S. In the FTIR spectrum of G, the vibration band of Zr−OH occurred at $1230−800$ cm^{-1}, the vibration band of O−Zr−O occurred at 654 cm^{-1}, and the stretch vibration band of O−H in Zr−OH occurred at $3600−3300$ cm^{-1}. Both the above vibration bands existed in SG and SGA, indicating that the G and S were successfully mixed in the suppressant. After the addition of active component A, the absorption peak of the flexural vibration of NH$_4^+$ occurred at $1790−1230$ cm^{-1} and the absorption peak of the asymmetric stretching vibration of NH$_4^+$ occurred at $3260−2800$ cm^{-1}.

In the FTIR spectra before and after coal dust explosion (Figure 9), the vibration peaks of the chemical structure in the
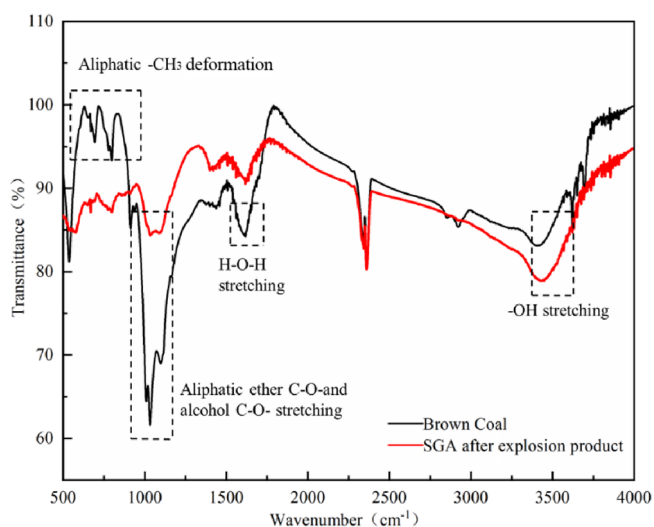

Figure 9. Infrared spectra of the explosion suppressant before and after explosion.

lignite specimen mainly occurred at $1600−600$, $3000−2280$, and $3700−3300$ cm^{-1}.[43] The functional groups mainly consisted of the C−H bonds in olefins and in aromatic hydrocarbons as well as hydroxyl groups. The peaks at $1700−1510$ cm^{-1} corresponded to the vibration of the C=C bonds in the aromatic hydrocarbon. With the addition of the SGA suppressant, the FTIR spectrum after coal dust explosion showed that the intensity of the C−H vibration peaks

Figure 7. TG-DTG curves of (a) S, (b) SG, and (c) SGA.

caused by a small amount of aluminum oxide in S acting as a stabilizer of zirconium oxide. In stage 5, from 360 to 550 °C, there was nearly no change in weight.

In the Fourier-transform infrared (FTIR) spectroscopy analysis of S shown in Figure 8a, vibration bands of Si−O$_4$ and Al−O$_4$ appeared at $1320−720$ cm^{-1}, the stretch vibration band of O−H in aluminosilicate Si−OH and Al−OH occurred at $3600−3200$ cm^{-1}, and the stretching vibration peak of Si−H occurred at $2360−2270$ cm^{-1}. This vibration band also

decreased significantly. Additionally, the intensity of oxygen-containing functional groups at 1098 cm^{-1} significantly decreased, the intensity of the peak associated with water at 1602 cm^{-1} slightly decreased, and the intensity of the hydroxyl vibration peak at 3429 cm^{-1} decreased. The FTIR spectrum before and after the addition of suppressant showed that the chemical structures in the lignite specimen, including olefin, aromatic hydrocarbon, oxygen-containing functional groups, and hydroxyl groups, participated in the lignite explosion reaction.

2.2. Flame Propagation Inhibition. *2.2.1. Influence of S, G, and SG on the Flame Propagation Inhibition of Coal Dust.* Figure 10 shows the flame suppression results with
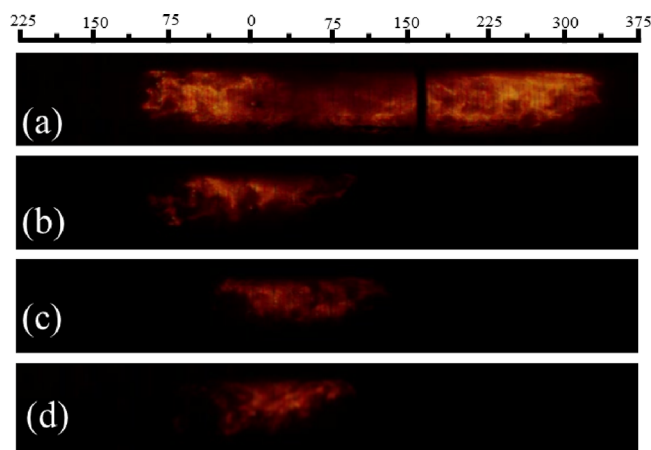

Figure 10. Flame suppression results with different suppressors. (a) Blank, (b) 20 wt % S, (c) 20 wt % G, and (d) 20 wt % SG (S/G = 1/1).

different suppressors. When the coal dusts contacted a heated platinum wire without a suppressant, the explosive flame rapidly diffused in the tunnel and reached a maximum length of 400 mm, which indicated that coal dust of lignite was strongly explosive, as shown in Figure 10a. With the addition of 20 wt % of S and G, the flame of the coal dust explosion was suppressed, as shown in Figure 10b,c, respectively. Under the same conditions, with the addition of a mixture of S and G, the maximum length of flame was about 100 mm. The decrease in maximum flame length in Figure 10d demonstrated that the SG had the best suppression effect.

2.2.2. Influence of Different SG Contents on the Inhibition of Flame Propagation of Coal Dust. Figure 11a−e shows the flame suppression diagram of the increase from 10 to 30 wt %. As the amount of SG increased in the explosion suppression test, the flame of coal dust explosion was shortened. With the addition of 15 wt % of SG, the length of the flame was 250 mm, which was shortened by nearly 40% due to the effect of explosion suppression. With the addition to 30 wt %, the flame basically disappeared, illustrating that the coal dust explosion was completely suppressed.

2.2.3. Inhibition of Coal Dust Flame Propagation with Different Ratios of S and G. As shown in Figure 12a, the total length of the flame from lignite reached 400 mm when no suppressant was present. Figure 12a−i showed the flame suppression diagram of waste molecular sieve and zirconia at different proportions with the increase in zirconia. The length of the flame showed a trend of first shortening and then increasing with the decrease in G. As shown in Figure 12g,
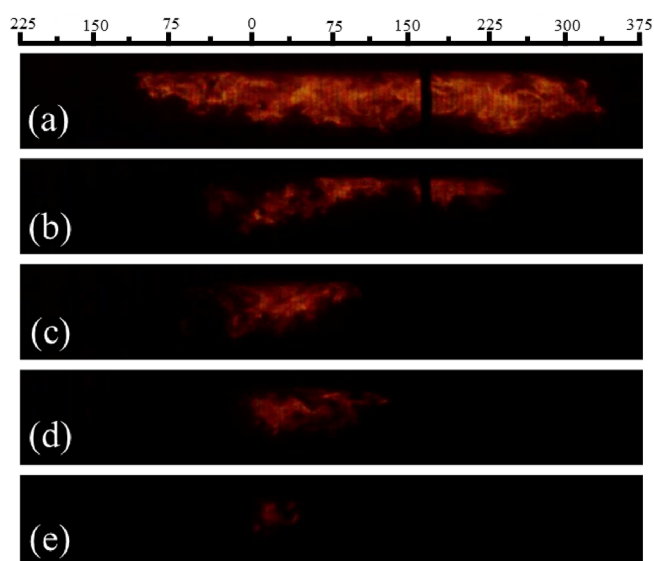

Figure 11. Flame suppression graph of coal dust with different added amounts of waste molecular sieve and zirconia with the S/G = 1/1. (a) 10 wt % of SG, (b) 15 wt % of SG, (c) 20 wt % of SG, (d) 25 wt % of SG, and (e) 30 wt % of SG.
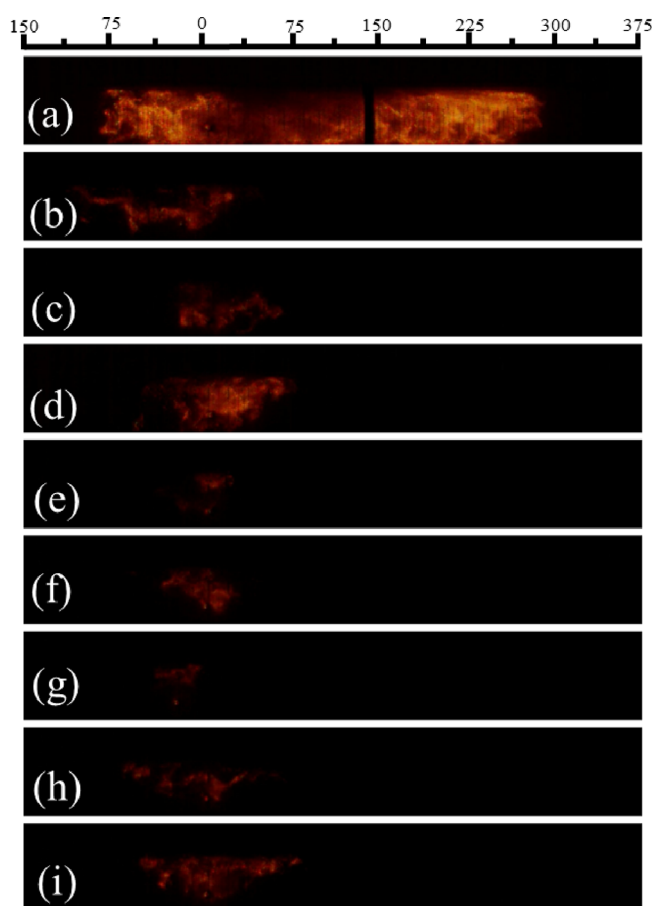

Figure 12. Flame suppression diagram of waste molecular sieve and zirconia at different ratios of 20 wt %. (a) Blank, (b) S/G = 5/1, (c) S/G = 3/1, (d) S/G = 1/1, (e) S/G = 1/3, (f) S/G = 1/5, (g) S/G = 1/7, (h) S/G = 1/9, and (i) S/G = 1/11.

when the S/G mass ratio was 1/7, the coal dust explosion was effectively suppressed.

2.3. Performance of Coal Dust Explosion Suppression for the SGA Suppressant. As shown in Figure 13, it can be
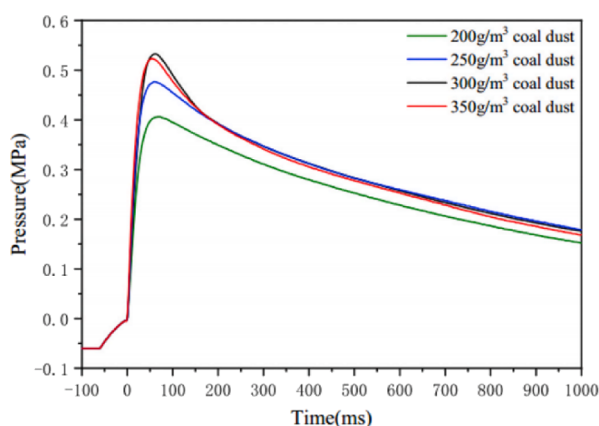

Figure 13. Coal dust explosion characteristic experiment.

seen from the experimental results that when the concentration of coal dust explosion is 300 g/m³, coal dust explosion has the maximum explosion pressure and the maximum explosion pressure rising speed. Therefore, 300 g/m³ (6g of coal dust) was selected as the best concentration for experimental testing.

The 20 L spherical device used in the explosion experiment obtains the maximum explosion pressure P_{max} and the maximum explosion pressure rise rate $(dP/dt)_{max}$ as shown in Figure 14.
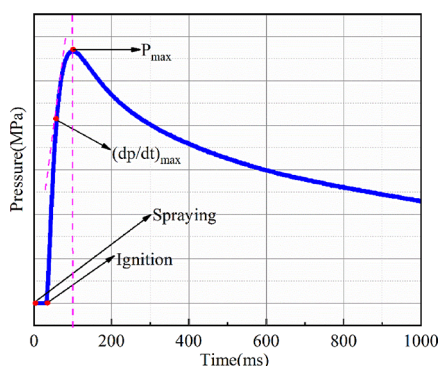

Figure 14. Diagram of the explosion pressure curve.

The curves of pressure changing after the addition of suppressants with different mass ratios show that with the increase in suppressant, the pressure peaks of explosion decreased continuously, the rates of pressure increase continuously slowed, and the rates to reach the peak also continuously slowed, as shown in Figure 15. These changes occurred because the higher the mass ratio of the suppressant was, the greater was the mass concentration of the suppressant, and the explosion suppression effect was improved. The pressure curve of an explosion with an explosion concentration of 300 g/m³ of lignite was used. The maximum explosion pressure P_{max} was 0.56 MPa, the increased rate of maximum explosion pressure $(dP/dt)_{max}$ was 19.336 MPa/s, and the time to reach the peak was 30 ms. As the amount of added suppressant rose to 40 and 50 wt %, the rate of rise of the pressure curve and the peak both significantly decreased. When the suppressant content was 60 wt %, the gradient of the curve decreased, with P_{max}, $(dP/dt)_{max}$, and time to peak values of
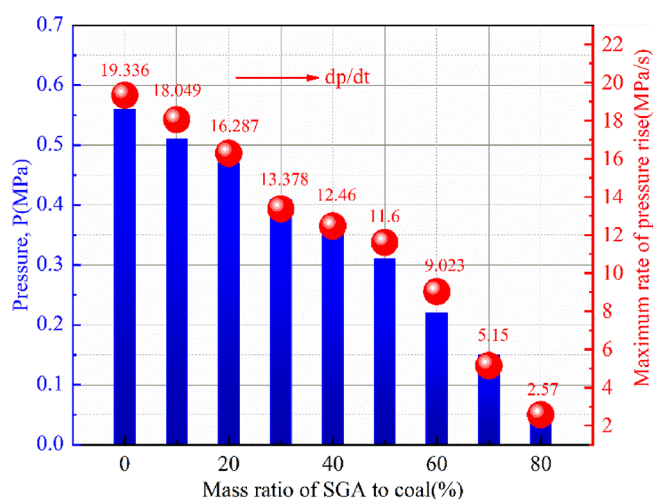

Figure 15. Influence of different SGA additions on coal dust explosion parameters.

0.22 MPa, 9.023 MPa/s, and 60 ms, respectively. Compared with the baseline curve, the P_{max} and $(dP/dt)_{max}$ decreased by 39%, and the time to reach the peak doubled. When the content of suppressant was increased to 70 wt %, the P_{max}, $(dP/dt)_{max}$, and time to peak values were 0.15 MPa, 5.15 MPa/s, and 80 ms, respectively. Increasing the suppressant content to 80 wt %, the coal dust explosion was basically suppressed, with P_{max}, $(dP/dt)_{max}$, and time to peak values of 0.06 MPa, 2.57 MPa/s, and 100 ms, respectively.

2.4. Mechanism of Explosion Suppression. In the paper, S was mixed with mesoporous ZrO_2 to prepare the suppressant with high added value, which could provide important security for coal industry and realize the green reuse of waste molecular sieves. At the same time, A was used as the active component for explosion suppression, and it was loaded on the mesoporous carrier to prevent the aggregation of A, increase its dispersity, establish a physical and chemical synergistic effect, and improve its effectiveness as an explosion suppressant. The mechanism of explosion suppression of the novel suppressant mainly involved three main effects, as illustrated in Figure 16.

(1) The physical effect. A, separated from the mesoporous carrier, absorbed the heat at a high temperature, decomposed, and generated NH_3 and CO_2 gas, which attenuated the oxygen concentration in the explosion area. After the micro-mesoporous (SG) particles were heated, S and G coated the surface of the unexploded coal dust particles, which segregated the particles and caused them to avoid the reaction of the explosion. Dehydration occurred in the process of heating S, with adsorbed H_2O absorbing the heat and evaporating, which had an effect on the cooling effect. As presented in Table 1 and Figure 2, SG had a relatively large specific surface area and a specific pore structure that resulted in the good adsorption performance of the suppressant and fully contacted and adsorbed the free radicals in the explosion chain reaction, causing the chain reaction to stop.

(2) The chemical effect. As shown in Figure 3, S contained elements such as Fe and Ni, and the existence of element Fe consumed some of the OH· in the explosion reaction to stop the chain reaction. Additionally, as a
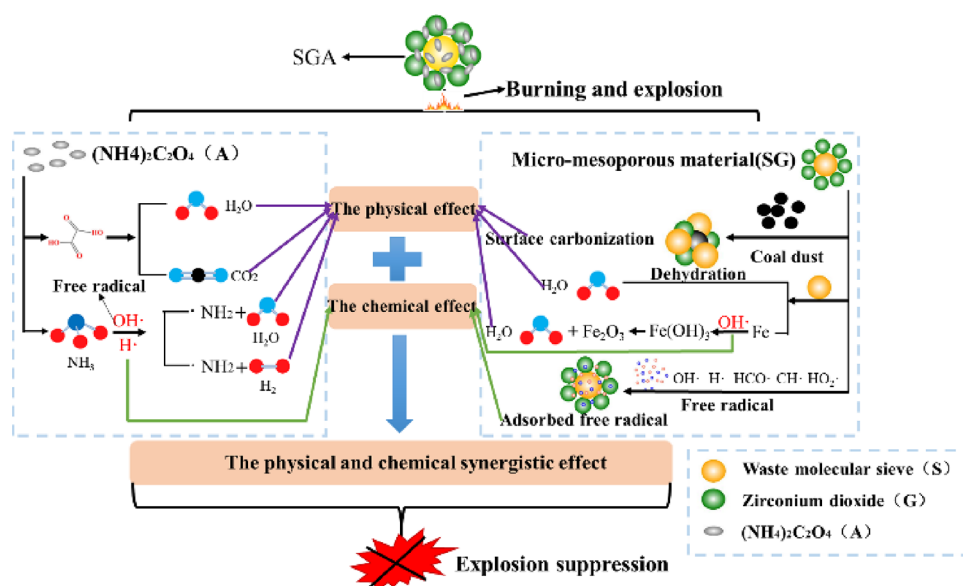
Figure 16. Mechanism of coal dust explosion suppression for SGA.

decomposition product of A, NH$_3$ was generated before CH$_4$, which reacted with the active free radical OH· and H· to generate ·NH$_2$, H$_2$, and H$_2$O first, and thus the chain reaction of coal dust explosion was stopped.

(3) The physical and chemical synergistic effect. The cooling effect of A in the suppressant was achieved by decomposition and heat absorption, and the mesoporous carrier had a special pore structure and relatively large specific surface area, which resulted in a good physical explosion suppression effect. At the same time, the Fe and Ni in the suppressant and the decomposition product NH$_3$ could react with the active free radicals of the explosion to play a chemical effect. The suppressant simultaneously achieved the above physical and chemical synergistic effect with high efficiency, which demonstrated good explosion suppression performance.

3. CONCLUSIONS

In this paper, the microporous waste molecular sieve and zirconium dioxide were used to form a micro-mesoporous structure as the matrix, and the (NH$_4$)$_2$C$_2$O$_4$ was first loaded to realize the green recycling of waste molecular sieve to prepare a novel coal dust explosion suppressant with a micro-mesoporous structure. Physical inhibition mainly consists of a physical coating, physical endothermic cooling effect and gas inerting effect. The micro-mesoporous suppressant has a large specific surface area and good pore structure, which enhances the ability to adsorb free radicals of the explosive chain reaction. Fe and decomposition products NH$_3$ in the suppressant can react with active free radicals, which shows efficient chemical effects.

The suppressant has an irregular bulk shape, and each component was well dispersed in the novel suppressant, which was prepared by a dry mixing method. The specific surface area and total pore volume of SGA decreased with the loading of A due to the fact that the pore was gradually filled with A. In addition, A was first loaded into the micropore structure of the micro-mesoporous suppressant. Meanwhile, the active components dispersed uniformly and their aggregation problem was solved.

In the explosion reaction, the species that participated in the explosion reaction are mainly olefin, aromatic hydrocarbon, oxygen-containing functional groups, and hydroxyl groups. When the ratio of waste molecular sieve, zirconium dioxide, and (NH$_4$)$_2$C$_2$O$_4$ of suppressant is 1:7:2, it has the best inhibitory effect in explosion suppression. The suppressant performance increases with the increase in its addition. When the addition amount of suppressant is 70 wt %, the coal dust explosion loses the ability to continue to expand.

In the end, the physical and chemical synergistic suppression mechanism of the micro-mesoporous suppressant based on waste molecular sieve is proposed, which reveals the reason how the novel suppressant plays a role in efficient explosion suppression.

4. EXPERIMENTAL SECTION

4.1. Preparation of the Explosion Suppressant. Zirconium dioxide (G) and (NH$_4$)$_2$C$_2$O$_4$ (A) were from Qingdao Jingke Chemical Reagent Company. The brown coal was from Pingzhuang, Inner Mongolia, and it was selected and screened by a 200-mesh standard sieve, and the experiment was carried out with a particle size less than 75 μm. Figure 17 and Table 2 show particle size analysis of pulverized and industrial analysis. Figure 17 shows that the coal dust particle size distribution is concentrated in 74.3 μm. Table 2 shows that the volatile matter and fixed carbon content in pulverized coal is relatively high.

The specific preparation process is as follows: First, the waste molecular sieve (S) was calcined at 500 °C for 4 h so as to remove the residual oil. After that, molecular sieve was mixed with zirconium dioxide according to a mass ratio of 1/7 to obtain a waste molecular sieve-based micro-mesoporous material (SG). Then, 20 wt % of the active ingredient (NH$_4$)$_2$C$_2$O$_4$, it was dissolved in deionized water, and the solution was dispersed in an ultrasonic cleaner for 30 min. The temperature of the water bath was 30 °C. Finally, the waste molecular sieve-based micro-mesoporous material (SG) was added to the above (NH$_4$)$_2$C$_2$O$_4$ solution, stirred evenly, and, under the condition of a water bath temperature of 30 °C, ultrasonically dispersed and loaded for 30 min so that the

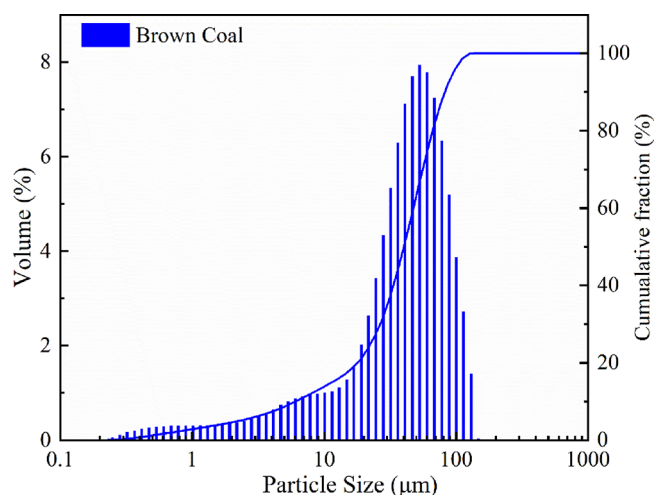Figure 17. Particle size distribution of coal dust.

Table 2. Proximate Analysis of Brown Coal

sample	proximate(%)			
	M_{ad}	A_{ad}	V_{ad}	FC_{ad}
brown coal	6.31	17.01	32.8	43.88

active molecules and the carrier were fully dispersed and contacted. After that, a turbid liquid was obtained. The turbid liquid was allowed to stand for 12 h to form a precipitate and dried at 30 °C for 12 h. The precipitate was taken out, crushed, and sieved to obtain a micro-mesoporous composite powder explosion suppression material (SGA) based the waste molecular sieve. The specific preparation process is shown in Figure 18.
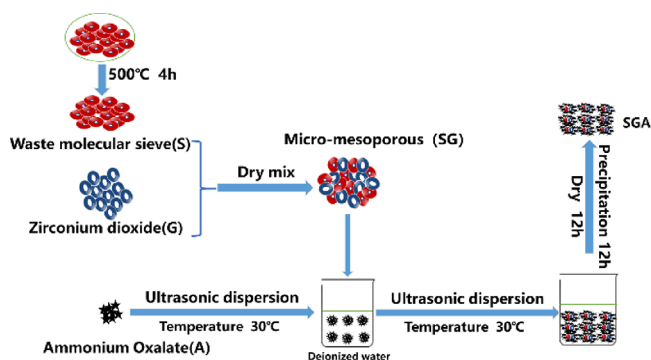

Figure 18. Composite powder SGA preparation process.

4.2. Laboratory Equipment. Through the dust explosion flame propagation test system, the coal dust flame suppression experiment was carried out, as shown in Figure 19. First, 1.0 g of coal powder and different quality explosion suppressant samples were placed in the sample tube, and the sample tube was installed firmly to prevent air pressure from rushing. Then, the platinum wire was moved from the small hole at the back of the pipe and heated up to 1100 ± 1 °C, and the powder spraying pressure was set to 0.05 MPa. In this state, the start switch was pressed to spray the pulverized coal into the pipe while high-speed photography was used to record the longest state of the flame image, and each group of experiments was performed 3 times in parallel.
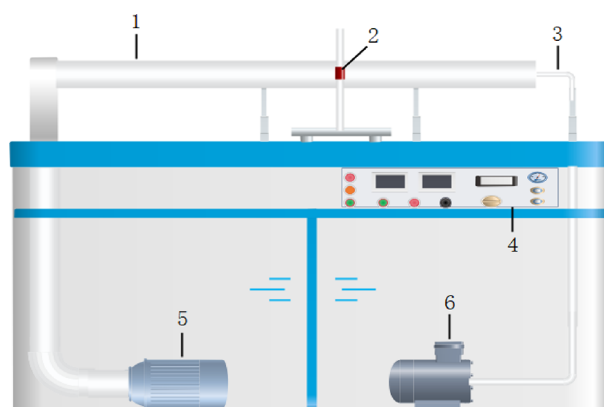
1 Glass tube 2 Platinum heater 3 Sample tube 4 Control System

5 Vacuum cleaner 6 Air compression

Figure 19. Dust explosion flame propagation test system.

The 20 L spherical explosion test system was used to test the coal dust suppression performance, as observed in Figure 20. A
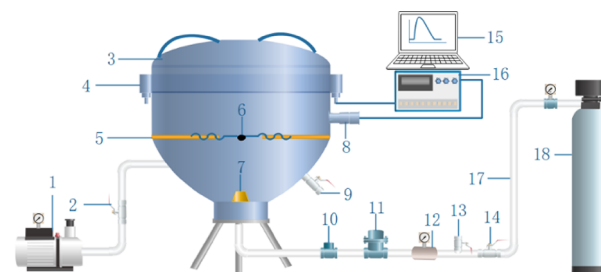
1. Vacuum pump 2. Valve 3. 20L spherical tank 4. Electrode connection line 5. Electrode outlet valve 6. Ignition tip 7. Powder spraying head 8. Pressure Sensor 9. Outlet valve 10. Dust storage bin 11. Solenoid valve pressure 12. High pressure gas tank 13. Control valve 14. Intake valve 15. Computer 16. Explosion test system 17. High-pressure gas pipeline 18. High pressure air tank

Figure 20. Twenty-liter spherical explosion test system.

10 KJ chemical ignition tip was used in the coal dust suppression test, a 60 ms ignition delay was set, and 6 g of pulverized coal and explosion suppressants of different qualities were mixed and added into the dust storage bin. The ignition tip was placed, and the tank was sealed. The spraying pressure of the solenoid valve was set to 2 MPa, the tank was vacuumed to −0.06 MPa through the vacuum pump, and the valve was closed to ensure that the experimental device was completely sealed. The device was started, and the sample was sprayed into the tank at a pressure of 2 MPa to form a dust cloud, which exploded using the ignition head. The explosion pressure curve was obtained through the pressure sensor. The maximum explosion pressure P_{max}, the maximum pressure rise rate $(dP/dt)_{max}$, and the time of reaching the pressure peak were recorded.

■ AUTHOR INFORMATION

Corresponding Author

Jinshe Chen − College of Safety and Environmental Engineering, Shandong University of Science and Technology, Qingdao 266590, China; Mine Disaster Prevention and Control-Ministry of State Key Laboratory Breeding Base, Shandong University of Science and Technology, Qingdao 266590, PR China; ⓞ orcid.org/0000-0003-1117-2185; Phone: + 86-18765262861; Email: skd1643@sdust.edu.cn

Authors

Yansong Zhang − College of Safety and Environmental Engineering, Shandong University of Science and Technology, Qingdao 266590, China; Mine Disaster Prevention and Control-Ministry of State Key Laboratory Breeding Base, Shandong University of Science and Technology, Qingdao 266590, PR China

Kun Chen − College of Safety and Environmental Engineering, Shandong University of Science and Technology, Qingdao 266590, China; ⓞ orcid.org/0000-0001-6023-4712

Junjie Yang − College of Safety and Environmental Engineering, Shandong University of Science and Technology, Qingdao 266590, China

Zhichao Pan − College of Safety and Environmental Engineering, Shandong University of Science and Technology, Qingdao 266590, China

Wenxi Shi − College of Safety and Environmental Engineering, Shandong University of Science and Technology, Qingdao 266590, China

Xiangbao Meng − College of Safety and Environmental Engineering, Shandong University of Science and Technology, Qingdao 266590, China; Mine Disaster Prevention and Control-Ministry of State Key Laboratory Breeding Base, Shandong University of Science and Technology, Qingdao 266590, PR China; ⓞ orcid.org/0000-0002-9290-5864

Xinyan Zhang − College of Safety and Environmental Engineering, Shandong University of Science and Technology, Qingdao 266590, China; Mine Disaster Prevention and Control-Ministry of State Key Laboratory Breeding Base, Shandong University of Science and Technology, Qingdao 266590, PR China

Min He − College of Safety and Environmental Engineering, Shandong University of Science and Technology, Qingdao 266590, China; Mine Disaster Prevention and Control-Ministry of State Key Laboratory Breeding Base, Shandong University of Science and Technology, Qingdao 266590, PR China

Complete contact information is available at:
https://pubs.acs.org/10.1021/acsomega.1c04791

Notes

The authors declare no competing financial interest.

■ ACKNOWLEDGMENTS

■ REFERENCES

(1) Bind, V. K.; Roy, S.; Rajagopal, C. A reaction engineering approach to modeling dust explosions. *Chem. Eng. J.* **2012**, *207-208*, 625−634.

(2) Cao, W.; Xu, S.; Liang, Q.; Pan, F.; Rao, G. Flame propagation characteristics in coal dust explosion. *Explos. Shock Waves* **2014**, *34*, 586−593.

(3) Zhu, Y.; Wang, D.; Shao, Z.; Xu, C.; Zhu, X.; Qi, X.; Li, F. A statistical analysis of coalmine fires and explosions in China. *Process Saf. Environ. Prot.* **2019**, *121*, 357−366.

(4) Liu, T.; Li, Y.; Luo, H. Experimental study on the variation of explosive pressure characteristics of coal dust with different metamorphic degrees. *Explos. Shock Waves* **2019**, *39*, 158−165.

(5) Xiu, Z.; Nie, W.; Yan, J.; Chen, D.; Cai, P.; Liu, Q.; Du, T.; Yang, B. Numerical simulation study on dust pollution characteristics and optimal dust control air flow rates during coal mine production. *J. Cleaner Prod.* **2020**, *248*, 119197.

(6) Bao, Q.; Nie, W.; Liu, C.; Zhang, H.; Wang, H.; Jin, H.; Yan, J.; Liu, Q. The preparation of a novel hydrogel based on crosslinked polymers for suppressing coal dusts. *J. Cleaner Prod.* **2020**, *249*, 119343.

(7) Huang, Y.; Dai, X.; Cao, W. Experimental study on suppression of coal dust explosion by dihydrogen phosphate and SiO_2 powder. *China Saf. Sci. J.* **2013**, *23*, 57−61.

(8) Wang, Q.; Wang, E.; Chen, X. Flame propagation pressure and temperature characteristics of gas explosion in pipeline. *J. Cent. South Univ.* **2020**, *51*, 239−247.

(9) Chen, L.; Li, P.; Liu, G.; Cheng, W.; Liu, Z. Development of cement dust suppression technology during shotcrete in mine of China-A review. *J. Loss Prev. Process Ind.* **2018**, *55*, 232−242.

(10) Hua, Y.; Nie, W.; Liu, Q.; Peng, H.; Wei, W.; Cai, P. The development and application of a novel multi-radial-vortex-based ventilation system for dust removal in a fully mechanized tunnelling face. *Tunnelling and Underground Space Technology.* **2020**, *98*, 103253.

(11) Zhou, L.; Ren, X.; Zhang, X. Summary of China's coal-to-oil industrial policy. *Chem. Ind. Eng. Prog.* **2012**, *31*, 2207−2212.

(12) Wei, Q.; Zhang, Y.; Chen, K.; Liu, B.; Meng, X.; Zhang, X.; Chen, H.; Chen, J. Preparation and performance of novel APP/NaY−Fe suppressant for coal dust explosion. *J. Loss Prev. Process Ind.* **2021**, *69*, 104374.

(13) Liu, Q.; Nie, W.; Hua, Y.; Yin, S.; Guo, L.; Peng, H.; Ma, H.; Zhou, W. Investigation of efficient dust control strategy for construction tunnels: Ventilation system's implications for cleaner production. *Building and Environment.* **2020**, *180*, 107032.

(14) Liu, W.; Mu, C. Numerical simulation of cavity wave suppression mechanism and experimental study on explosion suppression with coupled detonator. *J. Vib. Shock* **2020**, *39*, 88−95.

(15) Pei, B.; Yu, M.; Chen, L.; Zhu, X.; Yang, Y. Experimental study on the synergistic inhibition effect of nitrogen and ultrafine water mist on gas explosion in a vented duct. *J. Loss Prev. Process Ind.* **2016**, *40*, 546−553.

(16) Wen, X.; Guo, Z.; Wang, F.; Liu, M.; Pei, B. Experimental study on synergistic suppression of gas explosion by one-dimensional porous media and superfine water mist. *J. Saf. Environ.* **2020**, *20*, 539−547.

(17) Wang, X.; Zhang, Y.; Liu, B.; Liang, P.; Zhang, Y. Effectiveness and mechanism of carbamide/fly ash cenosphere with bilayer spherical shell structure as explosion suppressant of coal dust. *J. Hazard. Mater.* **2019**, *365*, 555−564.

(18) Cao, W.; Gao, W.; Peng, Y.; Liang, J.; Pan, F.; Xu, S. Experimental and numerical study on flame propagation behaviors in coal dust explosions. *Powder Technol.* **2014**, *266*, 456−462.

(19) Bi, M.; Dong, C.; Zhou, Y. Numerical Simulation of Flame Propagation in Methane-air Explosion in a Closed Long Tube. *J. China Coal Soc.* **2012**, *37*, 127−131.

(20) Fan, B.; Xie, B.; Zhang, X.; Li, H. Experimental study on explosion suppression process of inert dust. *Experiments and Measurements in Fluid Mechanics*; Oriprobe Information Services, Inc. 2001, *04*: 20−25.

(21) Cheng, F.; Deng, J.; Luo, Z.; Cai, Z. Experimental study on suppression of gas explosion by diatomite powder. *J. Min. Saf. Eng.* **2010**, *27*, 604−607.

(22) Yu, M.; Wang, T.; You, H. Study on the effect of thermal characteristics of powder material on gas explosion suppression. *J. China Coal Soc.* **2012**, *37*, 830−835.

(23) Yuan, B.; Tao, H.; Sun, Y. Study on synergistic suppression of methane explosion by porous mineral-ammonium polyphosphate. *China Saf. Sci. J.* **2021**, *31*, 41−46.

(24) Zhou, M.; Xiao, Y.; Chirag, B. Comparative investigation of CO_2/N_2 adsorption and diffusion on Na X, NaA and NaZSM-5 via molecular simulation. *RSC Adv.* **2020**.

(25) Liu, X.; Li, L.; Yang, T.; Yan, Z. Zeolite Y synthesized with FCC spent catalyst fines:Particle size effect on catalytic reactions. *J. Porous Mater.* **2012**, *19*, 133−139.

(26) Basaldella, E. I.; Palandino, J. C.; Solari, M. Exhausted fluid catalytic cracking catalysts as raw materials for zeolite synthesis. *Appl. Catal., B* **2006**, *66*, 186−191.

(27) Zhang, J.; Ding, H.; Zhang, Y.; Yu, C.; Bai, P.; Guo, X. An efficient one-pot strategy for synthesizing hierarchical aluminosilicate zeolites using single structure directing agent. *Chem. Eng. J.* **2018**, *335*, 822−830.

(28) Gao, Y.; Ru, Y.; Zhou, L.; Wang, X.; Wang, J. Preparation and characterization of chitosan-zeolite molecular sieve composite for ammonia and nitrate removal. *Adv. Compos. Lett.* **2018**, *27*, 185−192.

(29) Zhou, Y.; Wang, J.; Li, W.; Hu, X. Adsorption of CO_2 by Porous Molecular Sieves under Different Doping Modes of Triethylenetetramine. *World Sci. Res. Jl.* **2021**, *7*, 272.

(30) Chen, J.; Zhu, L.; Xiang, Y.; Xia, D. Effect of Calcination Temperature on Structural Properties and Catalytic Performance of Novel Amorphous NiP/Hβ Catalyst for n-Hexane Isomerization. *Catalysts* **2020**, *10*, 811.

(31) Zhu, Y. Current situation of waste catalyst recovery and utilization is reviewed. *Higher Vocational Studies of Changzhou Vocational Institute of Engineering*; CNKI Journal, 2010, 4: 44−50.

(32) Liu, L.; Ma, X.; Zhang, P. Overview of recovery and utilization of metal components in spent catalyst. *Industrial Safety and Environmental Protection*; Formosa Taffeta Co. 2012, *38*, 91−93+96.

(33) He, B. Analysis on the current situation of recovery and utilization of waste catalyst. *Chemical Enterprise Management.* 2016, *05*: 220.

(34) Ma, Y.; Zhao, H.; Tang, S.; Hu, J.; Liu, H. Synthesis of microporous/mesoporous composite molecular sieves and their CO_2 adsorption properties. *Acta Phys.-Chim. Sin.* **2011**, *27*, 689−696.

(35) Liu, S.; Ren, J.; Zhang, H.; Lv, E.; Yang, Y.; Li, Y.-W. Synthesis characterization and isomerization performance of micro/mesoporous materials based on H-ZSM-22 zeolite. *J. Catal.* **2016**, *335*, 11−23.

(36) Fedyna, M.; Śliwam, M.; Jaroszewska, K.; Trawczyński, J. Effect of zeolite amount on the properties of Pt/(AlSBA-15+Beta zeolite) micro-mesoporous catalysts for the hydroisomerization of n-heptane. *Fuel* **2020**, *280*, 118607.

(37) Ren, X.; Qu, R.; Liu, S.; Zhao, H.; Wu, W.; Song, H.; Zheng, C.; Wu, X.; Gao, X. Synthesis of zeolites from coal fly ash for removal of harmful gaseous pollutants: a review. *Aerosol Air Qual. Res.* **2020**, *20*, 1127−1144.

(38) Liu, S.; Li, J.; Zhao, N.; Wei, W.; Sun, Y. Methane and carbon dioxide reforming catalyzed by mesoporous Ni/CaO-ZrO$_2$ nanocomposite. *Chin. J. Catal.* **2007**, *11*, 1019−1023.

(39) Feng, M. *Preparation of mesoporous ZrO2 support and study on catalytic performance of gold nanoparticles supported*; Inner Mongolia Normal University. 2013.

(40) Gao, J. *Study on Surface Structure Regulation and Structure-activity Relationship of Y Molecular Sieves for Adsorption of Typical Volatile Organic Compounds*; Beijing University of Chemical Technology 2020.

(41) Ouyang, J. *Preparation and properties of zirconia based functional materials*; Central South University 2010

(42) Sun, Y.; Li, S. Study on the effect of additives on the thermal decomposition of AP/Al by infrared spectroscopy and thermal analysis. *Spectrosc. Spectral Anal.* **2008**, *01*, 75−79.

(43) Lin, S.; Liu, Z.; Zhao, E.; Qian, J.; Li, X.; Zhang, Q.; Ali, M. A study on the FTIR spectra of pre- and post-explosion coal dust to evaluate the effect of functional groups on dust explosion. *Process Saf. Environ. Protect.* **2019**, *130*, 48−56.